



Experimental investigation of buckling of thin-walled cylindrical shells subjected to combined bending and torsion

V. Ding¹, S. Torabian², X. Yun³,
A. Pervizaj⁴, S. Madsen⁵, B.W. Schafer⁶

Abstract

The objective of this paper is to provide and evaluate experimental results for buckling of thin cylindrical shells under combined bending and torsion appropriate for applications in steel wind turbine towers. Wind turbine towers are commonly made of steel cylindrical shells with large diameter-to-thickness ratios, making stability an essential concern. Towers are subject to complex loading including compression, bending, shear, and torsion, with the combination of bending and torsion at the top of the tower being a controlling load case. Though there have been a number of studies into the stability and design of cylinders subjected to isolated loading conditions (e.g. compression or bending), investigations into the structural response of thin-walled cylinders under combined bending and torsion remain scarce. To address the knowledge gap, an experimental study was carried out on the stability of steel cylinders under combined bending and torsion. A total of 48 cylinders with diameter-to-thickness ratios ranging between 127 and 320 were tested under varying bending and torsion combinations as commonly experienced in wind turbine towers. To gain further insight into the imperfection sensitivity of the shells, a 3D laser scanner was used to determine geometric imperfections of each test specimen prior to testing. The combined bending and torsion test setup, instrumentation, loading procedures, and structural response, including ultimate resistances, load-deformation characteristics and failure modes are reported. The test results are aimed to provide a firm basis for the validation of numerical models and development of advanced design approaches, such as the Reference Resistance Design, for cylindrical shells under combined bending and torsion. Future work will involve creating laboratory scale and full-scale wind turbine tower finite element models and providing improved guidance on combined bending and torsion demands.

1. Introduction

The stability of thin shells is a longstanding problem in structural stability. The high imperfection sensitivity of thin shells means accurately predicting their structural response is difficult. Any manufactured structure will always have imperfections, for shells lower failure loads are largely correlated to these imperfections. Standards of practice for a variety of structural engineering

¹ Ph.D. Candidate, Johns Hopkins University, USA <vding1@jhu.edu>

² Associate Research Scientist, Johns Hopkins University, USA <torabian@jhu.edu>

³ Lecturer, University of Sheffield, UK <x.yun@sheffield.ac.uk>

⁴ Lead Engineer, Vestas, Denmark <anpij@vestas.com >

⁵ Offshore Structures Specialist, Vestas, Denmark <sobgm@vestas.com>

⁶ Professor, Johns Hopkins University, USA <schafer@jhu.edu>

applications that utilize thin shells have been successfully established and utilized by engineers (e.g., ECCS, 2021, also see discussion in Rotter & Schmidt, 2013). However, each time engineers desire to move into new domains for thin shells they are once again faced with the extreme imperfection sensitivity in the structural response of these members and forced to develop adequate procedures for their design.

Today, one application for thin shells is the use of thin steel cylindrical tubes as supporting towers for wind turbines to produce renewable energy. Creating structurally efficient towers is one way of increasing tower heights, which provides turbines with higher and more consistent winds (Jay et al. 2016). However, using more material increases the carbon footprint of the tower itself, so sustainability goals also push towards the most efficient possible use of the material. That said, nothing is more wasteful than a structural tower failure, so structural efficiency must be balanced by structural reliability. Further complicating the problem are some of the specifics of wind turbine tower design: the balance between fatigue and stability driven failures, the relatively complex loading actions that can create unique bending and torsion demands on the same segment of tower, and additional considerations (Veritas 2002).

There has been extensive study of cylindrical shells under isolated loading conditions, e.g classic elastic stability work such as pure compression (Gere & Timoshenko 1961), pure bending (Seide & Weingarten 1961), or pure torsion (Donnell 1933). There are limited studies for combined load cases, as summarized in (Winterstetter & Schmidt 2002), but the literature is particularly scarce for combined bending and torsion. The combination of bending and torsion at the top of wind turbine towers can be a critical load case.

Codes and standards do cover the design of cylindrical shells subjected to combined loading. Eurocode 1993-1-6 (2021) has an interaction equation for combined loads of basic load cases, which are axial, shear, and hoop stresses, shown in Eq. 1,

$$\left(\frac{\sigma_{x,Ed}}{\sigma_{x,Rd}}\right)^{k_x} - k_i \left(\frac{\sigma_{x,Ed}}{\sigma_{x,Rd}}\right) \left(\frac{\sigma_{\theta,Ed}}{\sigma_{\theta,Rd}}\right) + \left(\frac{\sigma_{\theta,Ed}}{\sigma_{\theta,Rd}}\right)^{k_\theta} + \left(\frac{\tau_{x\theta,Ed}}{\tau_{x\theta,Rd}}\right)^{k_\tau} \leq 1 \quad (1)$$

where σ_x is axial stress, $\tau_{x\theta}$ is shear stress, σ_θ is hoop stress, subscript *Ed* means demand, subscript *Rd* means capacity, and $k_x, k_i, k_\theta, k_\tau$ are the buckling strength interaction parameters. These interaction parameters for cylindrical shells are have been established using both theoretical and experimental evidence (Rotter and Schmidt 2013). They were derived from simple interactions of basic load cases on cylindrical shells (Yamaki 1984; Schmidt and Winterstetter, 2004). This interaction equation intends to account for elastic buckling of thin shells and generally simplifies to von Mises yield criterion for thick shells. Herein, we have assumed σ_x applies to bending and not just axial compression. Eurocode does not explicitly state this, but to account for interaction, this assumption is a logical extension.

Another standard that covers combined loading is the AISC Load and Resistance Factor Design Specification for Steel Hollow Structural Sections (2000). This specification lists two interaction equations for load combinations that contain both normal and shear stresses from Felton & Dobbs (1967) and Schilling (1965). Several interaction equations for combined bending and torsion have also been proposed by Bruhn (1945), and Gerard & Becker (1957), all from experimental data.

Hill and Siebel (1951) studied the interaction between bending and torsion of thin tubes by solving equations numerically.

Recent work on combined bending and torsion of thin cylindrical shells, or studies on how their imperfection sensitivity affects this load case, are rare. To address the knowledge gap, an experimental study was performed on cylindrical shells under combined bending and torsion with applications to steel monopole wind turbine towers. A total of 48 cylinders were manufactured for testing with varying diameter-to-thickness (D/t) ratios and bending-to-torsion ratios comparable to ratios found in wind turbine towers. To gain further insight into the imperfection sensitivity of cylindrical shells under combined bending and torsion, a 3D laser scanner was used to measure geometric imperfections of each test specimen. These tests will later be compared with finite element models of the laboratory scale tubes followed by full scale wind turbine tower models utilizing laser scanning at full scale conducted as a companion effort.

2. Steel Monopole Wind Turbine Towers

DNV (2002) has detailed guidelines of the design of steel monopole wind turbine towers. Here we focus only on stability and ignore fatigue and other details required to fully design a tower. Discussion is limited to three major issues (1) the critical loading actions on the towers, (2) the overall slenderness of typical towers, and (3) tube geometries that are used for laboratory scale testing.

2.1 Critical Loading Actions

Fig. 1 illustrates the different loads wind turbine towers face. A typical tower under wind load is a cantilever with a few unique features at a particular moment in time. The blades can yaw so that they are in line with the wind but that does not happen instantly. This lack of alignment creates torsion. Wind on the blades and the tower result in large moment at the base, which often controls design. However, considering actual designs one will observe that the combination of torsion and moment controls the design of most of the top of the tower.

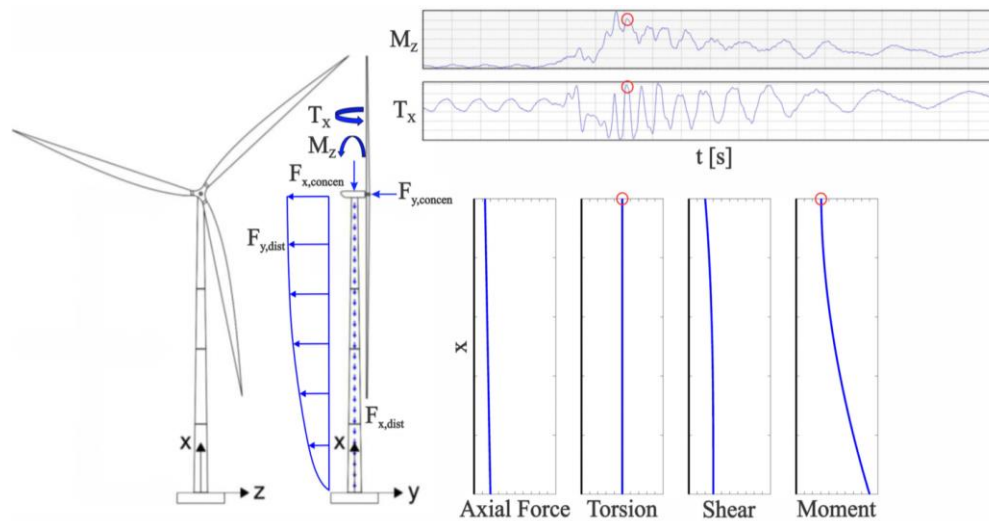


Figure 1: Time histories of the moment M_z and torsion T_x at the tower top during operational conditions with a coherent wind gust and directional change; instantaneous distributions of axial force, torsion, shear, and moment

2.2 Slenderness of Wind Turbine Towers

Fig. 2 and 3 show what turbine towers typically look like today. Fig. 3 provides a scaled drawing of a typical tubular steel tower. Turbine towers are slender, with heights over 100 meters and base diameters starting around 4 meters. Towers are built up from cans welded together, and as height increases, the can diameter decreases (and thickness changes), providing an overall taper. Typical cans are represented between dashed lines and are welded together to form segments, shown between solid lines. An entire tower is too long to be transported altogether, so segments are transported separately then connected by ring stiffeners, or flanges, on site. Flanges also increase tower strength by preventing ovalization. Fig. 2 shows data on 45 in-service onshore wind turbine towers. Each line represents D/t ratios of one turbine tower along its height. D/t ratios are low at the base of the tower to resist high moment demand. Moment demand decreases as you move up the height of the tower so D/t ratios increase as height increases. Then the D/t ratio decreases at the very top to deal with localized demands. The mean D/t ratio of every tower is 180. The mean of the maximum D/t ratio of each tower is 256, which is high. Ratio for length of a tower to its base diameter ratio is typically around 28.

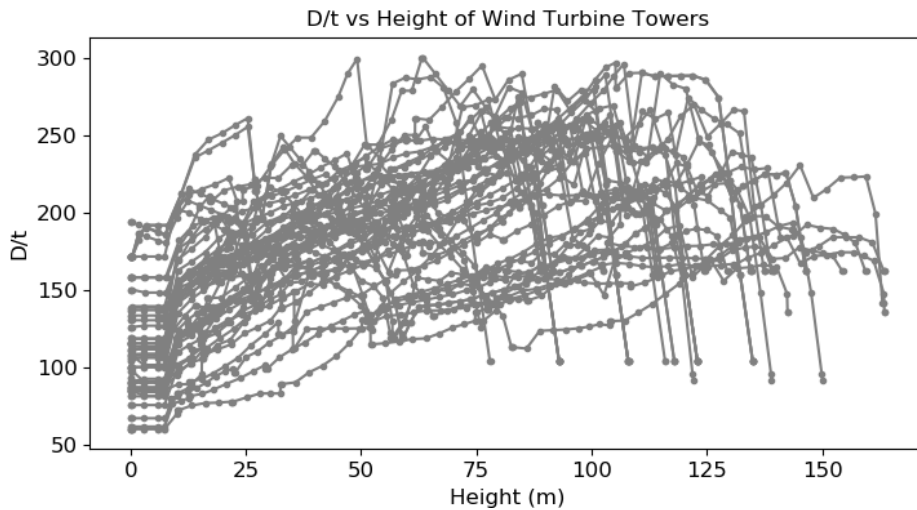


Figure 2: D/t variation across height of wind turbine towers

2.3 Tube geometries that are used for laboratory scale testing

Consistent with current practice for wind turbine towers and with an eye towards potentially using even more slender sections, we selected cylinders with D/t from 127 to 320 for our testing. Conveniently, and somewhat remarkably, Nordfab Ducting makes cylindrical steel members that are exactly in this range at a scale that can be tested in the laboratory.

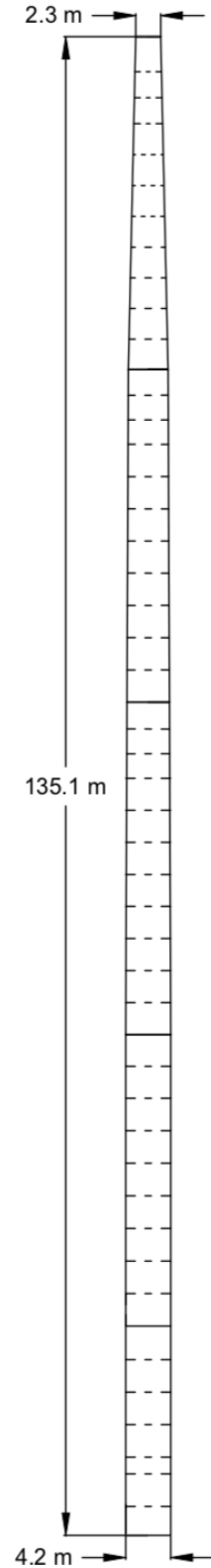


Figure 3: Scaled drawing of typical wind turbine tower

3. Eurocode and von Mises Formulas on Combined Bending and Torsion

3.1 von Mises yield criterion

Eq. 2 is the von Mises formula under bending and pure torsion

$$\frac{1}{\sqrt{2}} \sqrt{2\sigma_b^2 + 6\tau_T^2} = F_y \quad (2)$$

where σ_b is bending stress, τ_T is the torsional shear stress and F_y is yield stress. After converting from stresses to actions, one gets Eq. 3

$$\left(\frac{M}{M_y}\right)^2 + \left(\frac{T}{T_y}\right)^2 = 1 \quad (3)$$

where M is moment demand, T is torque demand, M_y is yield moment, and T_y is yield torque. Test results were compared with von Mises yield criterion using Eq. 3 as a basic baseline for comparison.

3.2 Eurocode interaction equation

Eq. 4 and 5 are derived from the Eurocode interaction formula from Eq. 1 using a combination of Eurocode's Annex D and Annex E. Annex E was introduced in the 2017 addendum. Comparison of test results with Eurocode was done using Eq. 5. Nominal strengths were used for comparison, meaning material factors were removed. Eq. 1 becomes Eq. 4 after removing terms involving hoop stress and introducing strength reduction factors.

$$\left(\frac{\sigma_{x,Ed}}{\chi_x F_y}\right)^{k_{ix}} + \left(\frac{\tau_{x\theta,Ed}}{\chi_\tau \tau_y}\right)^{k_{i\tau}} \leq 1 \quad (4)$$

Where χ_x and χ_τ are strength reduction factors, F_y is tensile yield stress, and τ_y is shear yield stress, where $\tau_y = \frac{1}{\sqrt{3}} F_y$. Eurocode uses plastic moment considering imperfections as the reference for peak bending strength rather than yield moment. After replacing F_y and converting from stress to actions, we obtain Eq. 5

$$\left(\frac{M}{\chi_x M_{r,pl,I}}\right)^{k_{ix}} + \left(\frac{T}{\chi_\tau T_y}\right)^{k_{i\tau}} \leq 1 \quad (5)$$

where $M_{r,pl,I}$ is the reduced reference plastic moment accounting for imperfections and the interaction coefficients k_{ix} and $k_{i\tau}$ are defined in Eurocode.

4. Experimental Tests on Cylindrical Shells Under Combined Bending and Torsion

Experiments on cylindrical shells under combined bending and torsion were conducted in the Thin-walled Structures Laboratory at Johns Hopkins University. Table 1 lists dimensions and loading configurations for each tube. There are 48 tubes in total; 4 different sized tubes and 12 of each size. Each size has 4 different torque-to-moment (T/M) loading ratios. T/M=0 implies bending only and T/M=1 implies an equal amount of torque and bending moment applied. All tubes were first laser scanned then tested in combined bending and torsion. The objective of these tests is to see their structural response, including ultimate resistances, load-deformation characteristics, and failure modes. These tests will later be compared with finite element models incorporating geometric imperfections from the laser scans.

Table 1: Summary of laboratory scale tubes with slenderness complementary to steel towers

Nominal Size	D ¹	t	L	D/t	L/D	Out-rigger	Moment arm	T/M	Number of Specimens
(mm)	(mm)	(mm)	(mm)			(mm)	(mm)		
100	100	0.79	300	127	3	149	449	0	3
100	100	0.79	300	127	3	149	449	0.33	3
100	100	0.79	300	127	3	149	449	0.66	3
100	100	0.79	300	127	3	149	449	1	3
150	151	0.79	453	191	3	149	602	1	3
150	151	0.79	453	191	3	149	602	0.66	3
150	151	0.79	453	191	3	149	602	0.33	3
150	151	0.79	453	191	3	149	602	0	3
200	202	0.79	606	256	3	149	755	0	3
200	202	0.79	606	256	3	149	755	0.33	3
200	202	0.79	606	256	3	149	755	0.66	3
200	202	0.79	606	256	3	149	755	1	3
250	253	0.79	759	320	3	149	908	1	3
250	253	0.79	759	320	3	149	908	0.66	3
250	253	0.79	759	320	3	149	908	0.33	3
250	253	0.79	759	320	3	149	908	0	3

1. D is outer diameter

4.1 Laser Scanning

Each tube was laser scanned before testing to record its geometric imperfections and gain a better understanding of its imperfection sensitivity. Laser scans provide higher precision and much more data than physical measurements. Fig. 4 provides a photo of a 250mm diameter tube in the lab's laser scanning rig (Zhao et al. 2015). Eurocode has three different fabrication quality classes depending on the severity of geometric imperfections. Class A is excellent quality, class B is high quality, and class C is normal quality. Eurocode determines fabrication quality by measuring dimple depths and out-of-roundness (deviation from circularity). Currently there are no standard procedures on how to process laser scanned data for measurements or how to determine fabrication quality with them. This discussion is ongoing and these tubes will later be classified with Eurocode's imperfection quality classes then used for creating finite element models of the laboratory scale tubes and compared with experimental results.



Figure 4: Laser scanner with a 250mm diameter tube

4.2 Experimental Test Setup

The tubes are manufactured by rolling up a thin rectangular sheet into a cylinder and seam welding where they meet. The tubes were then sent to a machine shop to weld end plates to both ends so they can be attached to the testing rig. A new testing rig was created in the lab to conduct these tests. Figure 5 provides a drawing and photo of the testing rig with a 250mm diameter tube loaded with $T/M=0.33$.

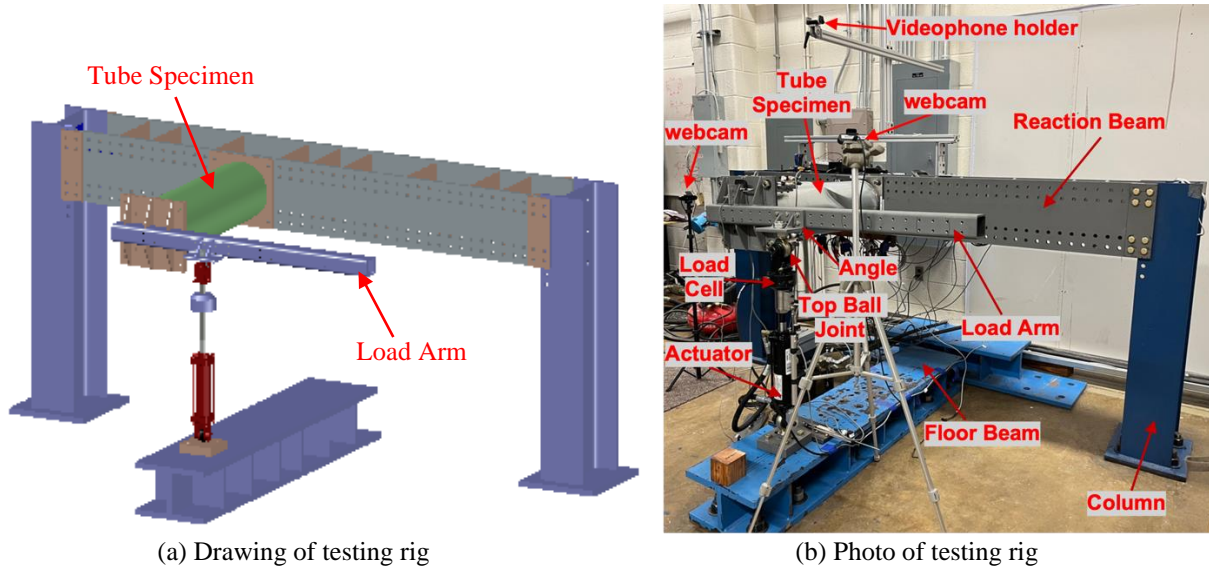


Figure 5: Testing rig setup for a 250mm tube loaded with $T/M=0.33$

The load arm is stiff and introduces eccentricity, providing torsion in addition to bending. The load is applied upward against gravity so that self-weight can be eliminated. The outrigger distance listed in Table 1 is the distance from the end of the tube to where the load is applied. This needs to be considered when calculating moment. To accommodate different T/M ratios, load is applied on different locations of the load arm. This is done by installing the tube at different locations along the reaction beam while the actuator stays in place. To accommodate different tube lengths, the actuator can be placed at different locations along the floor beam. The actuator is a 20.7 MPa (3000 psi) hydraulic cylinder with a load capacity of 65500 N (14,720 pounds). A load cell and

position transducer (PT) are attached to the actuator to record changes in load and control the crosshead displacement. Both ends of the actuator have clevis mounts attached to ball joints. The bottom ball joint is threaded into a plate which is bolted to the floor beam. The top ball joint is bolted to an angle which is bolted to the load arm. Three videos were recorded at different positions for each tube to capture the failure response during testing.

Figure 6 shows the coordinate system, position transducer locations, and angle definitions. Six position transducers are attached to the end plate. These PTs are used to calculate displacement and angle changes of the end plate during loading. The PTs are “spring loaded” and can stroke out or in up to 28 mm (1.125 in.) PT1 to PT4 are attached to bolts that connect the load arm to the end plate. PT5 and PT6 are placed on the floor and attached to heavy steel plates to prevent motion.

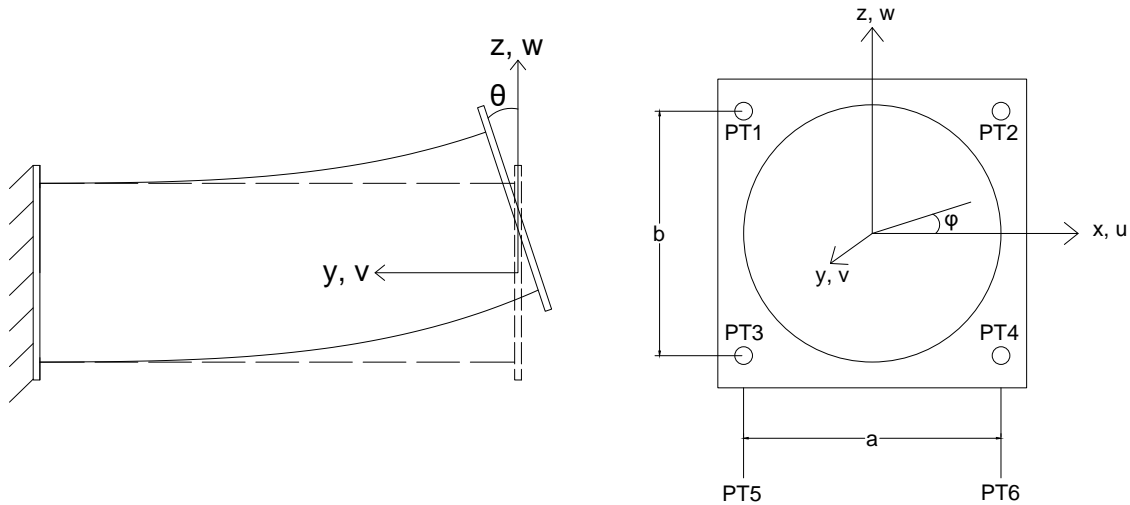


Figure 6: Coordinate system and PT locations

4.3 Experimental Procedure

To conduct a test, the tube and the loading angle on the load arm need to be installed in the correct location for a given T/M load combination. Custom LabVIEW programming is used to control the actuator’s stroke in a PID loop, and is utilized so that the actuator’s top clevis can be attached to the top ball joint using a shoulder bolt. The actuator is then moved in fine control, increasing or decreasing the stroke, such that the load reading is zeroed. Then the tube is loaded by extending the stroke at 0.025 mm/second (0.001 inch/second), pushing up on the load arm. Testing continues until the crosshead displacement is around 2 times the crosshead displacement at failure (peak load). Unloading occurs at 0.25 mm/second (0.01 inch/second) until the load reading is zero.

All controls and data collection were done through custom LabVIEW programming. The data collected includes load, crosshead displacement, and six PT displacements. Eq. 6-9 were used to find displacement and angles changes of the end plate from the PT data

$$v = \frac{\delta_1 + \delta_2 + \delta_3 + \delta_4}{4} \quad (6)$$

$$w = \frac{\delta_5 + \delta_6}{2} \quad (7)$$

$$\theta = \frac{\frac{\delta_1 + \delta_2}{2} - \frac{\delta_3 + \delta_4}{2}}{b} \quad (8)$$

$$\phi = \frac{\delta_6 - \delta_5}{a} \quad (9)$$

where δ_1 through δ_6 represent PT1 through PT6 displacements, a is the distance between PT5 and PT6, and b is the distance between PT1 and PT3.

5. Test Results

Table 1 provides nominal tube dimensions and the test matrix. A total of 48 tubes were tested with 4 different torque-to-moment (T/M) loading ratios and 4 different sizes: 250mm, 200mm, 150mm, and 100mm diameters. Three tubes were tested for each tube size and T/M combination. Photos of each tube at failure and plots of their results are provided in this section. Self-weight of the tube and weights of the end plates and load arm were taken into account (removed) in these plots. Figures for moment vs θ and torque vs ϕ are plotted until failure, which is peak load. Test results were compared with von Mises yield criterion using Eq. 3 and Eurocode's interaction formula using Eq. 5.

5.1 250mm Tube Results

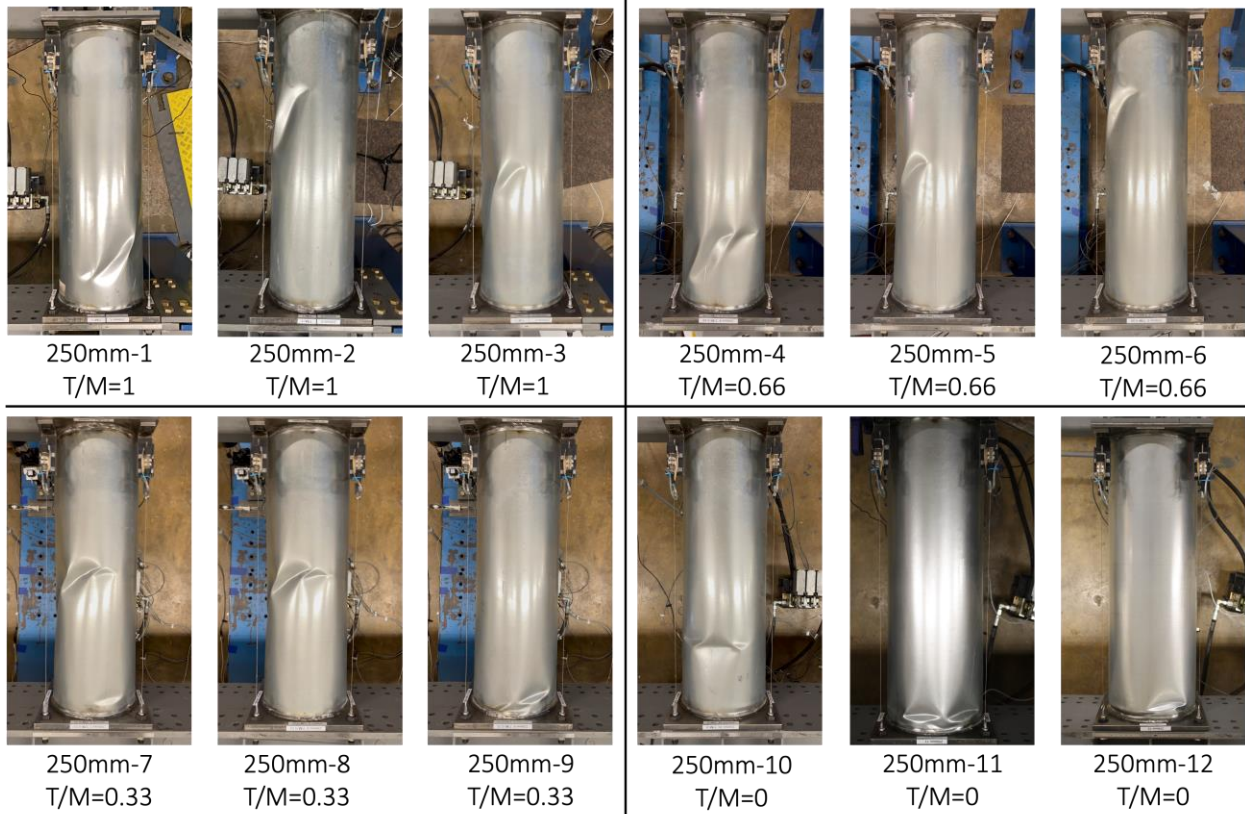
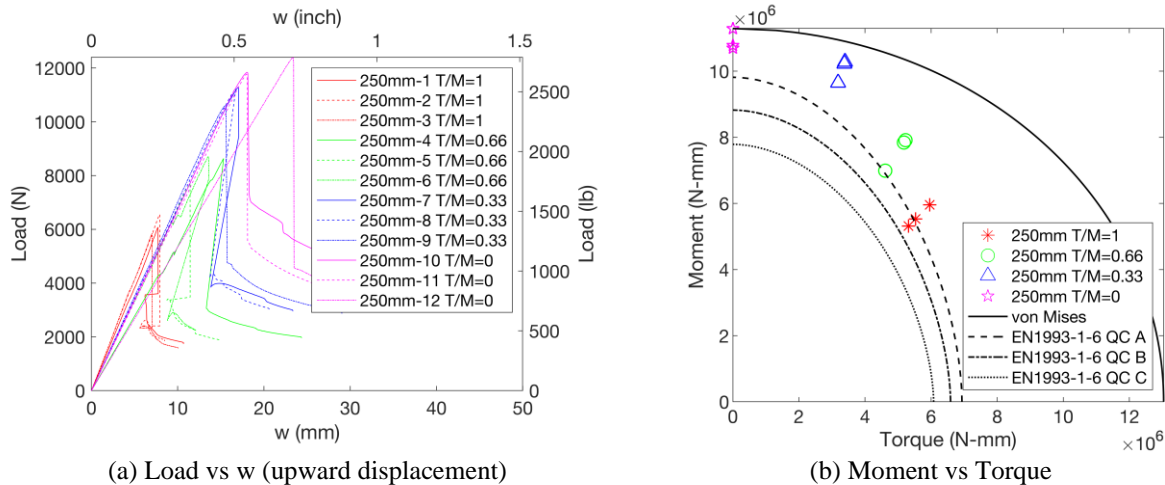


Figure 7: Photos of buckled 250mm tubes

Photos of the 250mm tubes right after failure are shown in Figure 7. The failure modes for bending only are different from failure modes with any torsion. In bending only, the tubes buckle with relatively short half waves around a cross section at failure near the reaction beam end, which had the highest moment. If there is any torsion, buckling waves form over a significant length of the section and at a diagonal angle across the tube.

Figure 8a shows load vs w , or upward plate displacement, of all 250mm diameter tubes. Buckling occurred essentially without prior indication for all tubes and load capacity dropped more than 50%. These tubes usually produced a loud popping sound at failure. As expected, tubes tested in bending only ($T/M=0$) had the highest failure load. As more torsion is added, failure load decreases. The load-deformation plots of the tubes originally had multiple changes in slope at the start of the tests. Based on later testing we now hypothesize that the testing rig columns were not well tied to the floor tie downs. This was fixed by extrapolating the elastic linear section to where load equals 0, then moving that point to the origin. The data for these large tubes have more scatter than the smaller tubes, but the elastic slopes are still similar. Figure 8b is an interaction diagram of moment vs torque, with the markers located at failure. The solid line is from von Mises and the other lines represent Eurocode calculations using fabrication quality classes A, B, and C. The data are in general agreement with Eurocode predictions. Figure 8c and 8d plot moment vs θ and torque vs ϕ of the data until failure, which is peak load. The theoretical bending stiffness is larger than bending stiffness from the test results, but the theoretical torsional stiffness matches well with the tests.



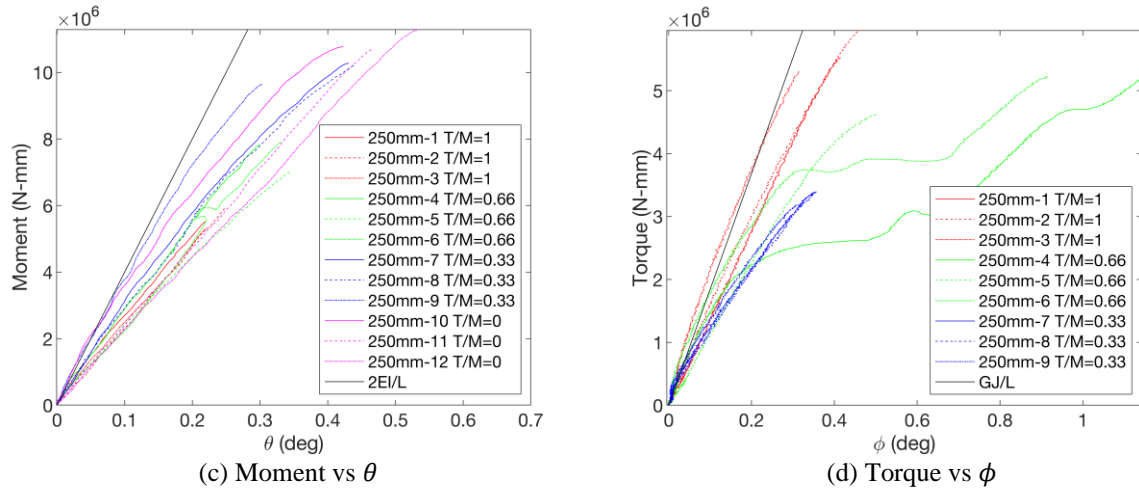


Figure 8: Results of 250mm tubes

5.2 200mm Tube Results

Fig. 9 has pictures of the 200mm diameter tubes after failure. The 200mm tubes have a D/t of 256. These tubes behaved similarly to the 250mm tubes. Like the 250mm tubes, the buckling shapes of the 200mm tubes under bending only ($T/M=0$) are different from tubes with any torsion. These tubes did not always produce a loud popping sound.

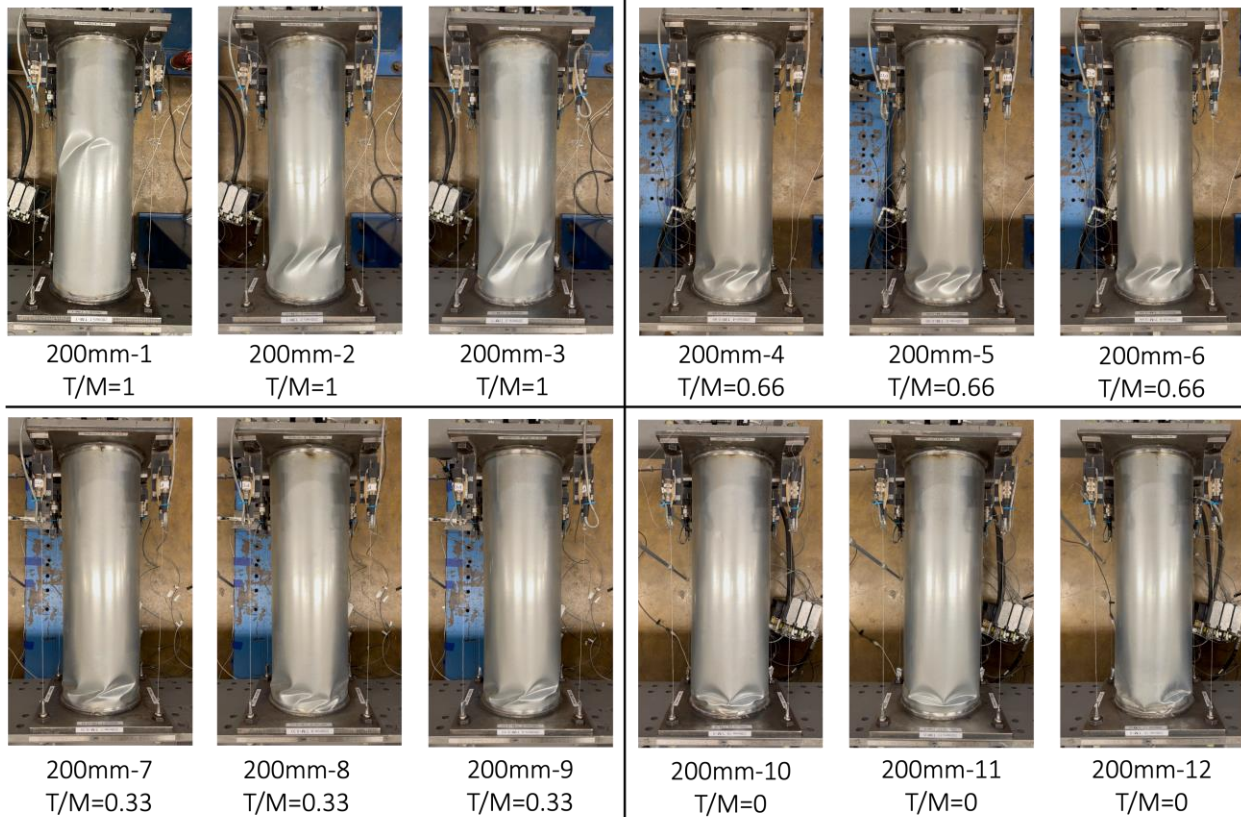


Figure 9: Photos of buckled 200mm tubes

Fig. 10 show the results of the 200mm diameter tubes. Fig. 10a shows load vs displacement of the 200mm tubes. Failure occurred with little warning but the drops in load are smaller here than for the 250mm tubes. Again, tubes tested in bending only had the highest failure loads, with failure load decreasing as more torsion is added. The data are in general agreement with Eurocode predictions. The 200mm tubes tested in only bending failed past yield. As the tubes get stockier, more will fail past yield. The theoretical bending stiffness is higher than bending stiffness of the test results, but the theoretical torsional stiffness matches well.

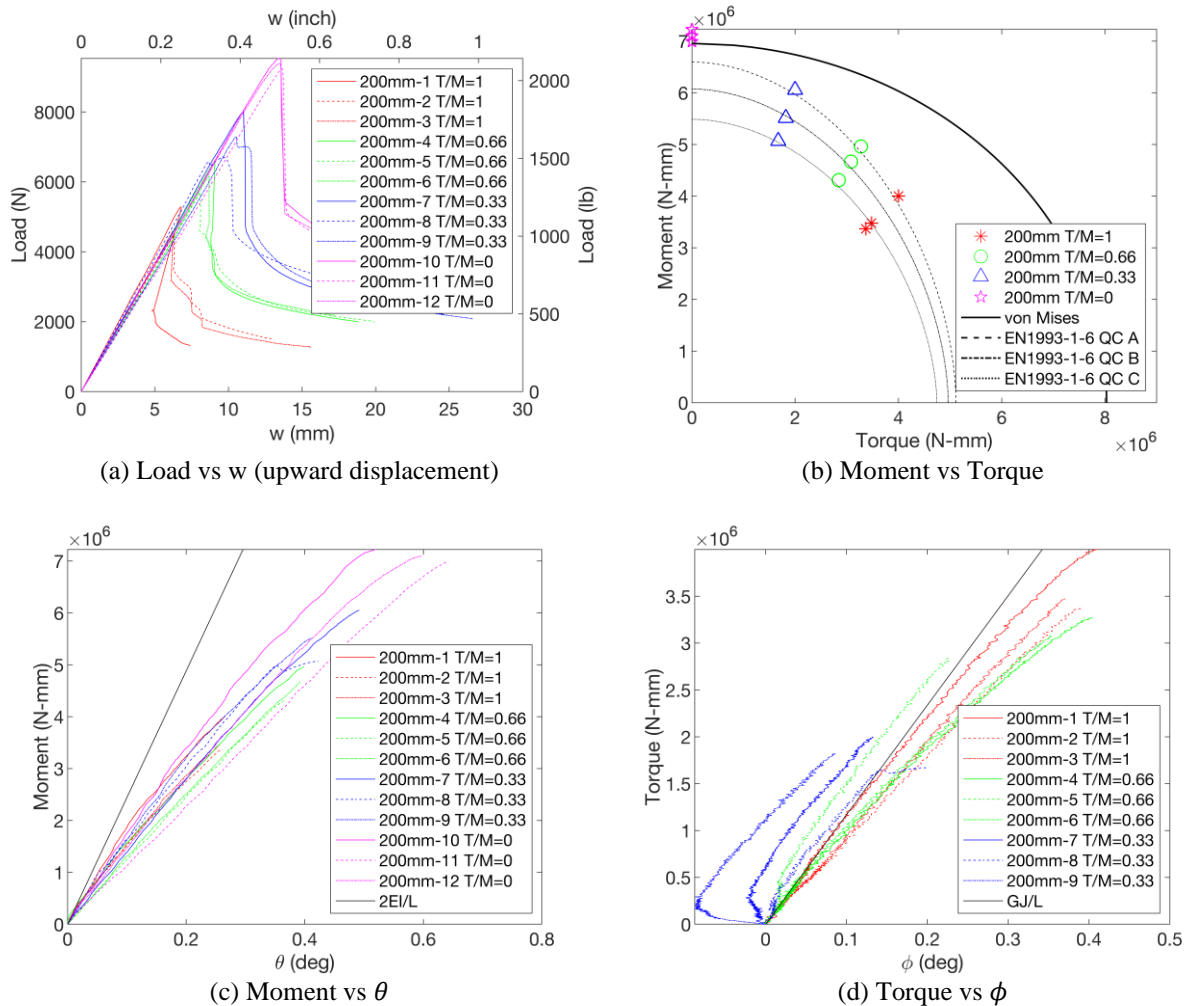


Figure 10: Results of 200mm tubes

5.3 150mm Tube Results

Fig. 11 has pictures of all 150mm diameter tubes after failure. The 150mm tubes have a D/t of 191. One tube is not shown here because it was not tested correctly. Some of these tubes, specifically tubes 7, 9, and 11, have different failure modes that were not seen in the larger tubes, where only one circumferential wave formed around a cross section at the base.

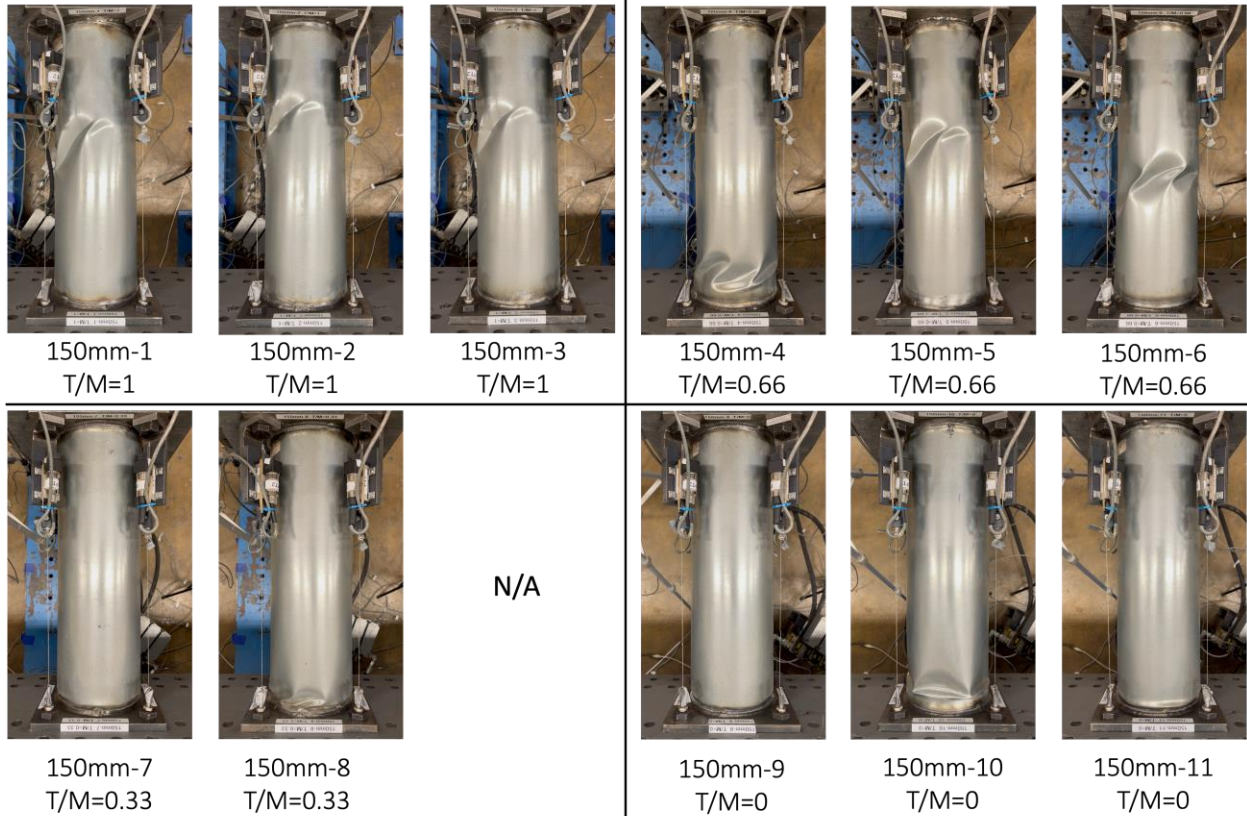
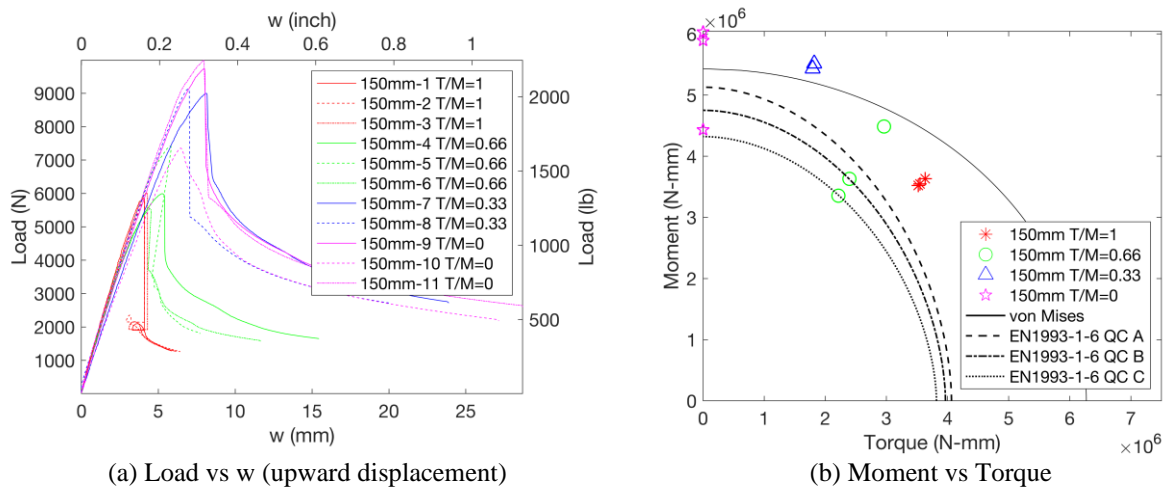


Figure 11: Photos of buckled 150mm tubes

Fig. 12 show the results for the 150mm tubes. In the load vs displacement plot, the data curves shortly before buckling, providing some warning before failure. However, the drops in load at failure are still significant. The theoretical bending and torsional stiffnesses match well and the data are in general agreement with Eurocode calculations. The 150mm tubes are stockier, so more failed past yield than the 200mm tubes.



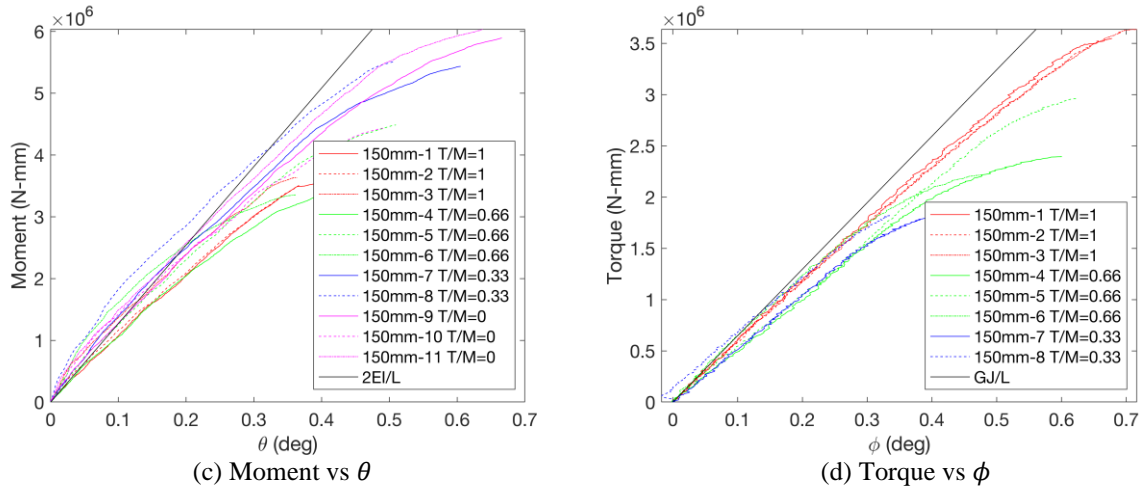


Figure 12: Results of 150mm tubes

5.4 100mm Tube Results

Fig. 13 has pictures of all 100mm diameter tubes, which are the stockiest tubes with the lowest D/t of 127. These tubes usually failed with one wave: A circumferential wave for tubes in bending only and at different angles for tubes with torsion.

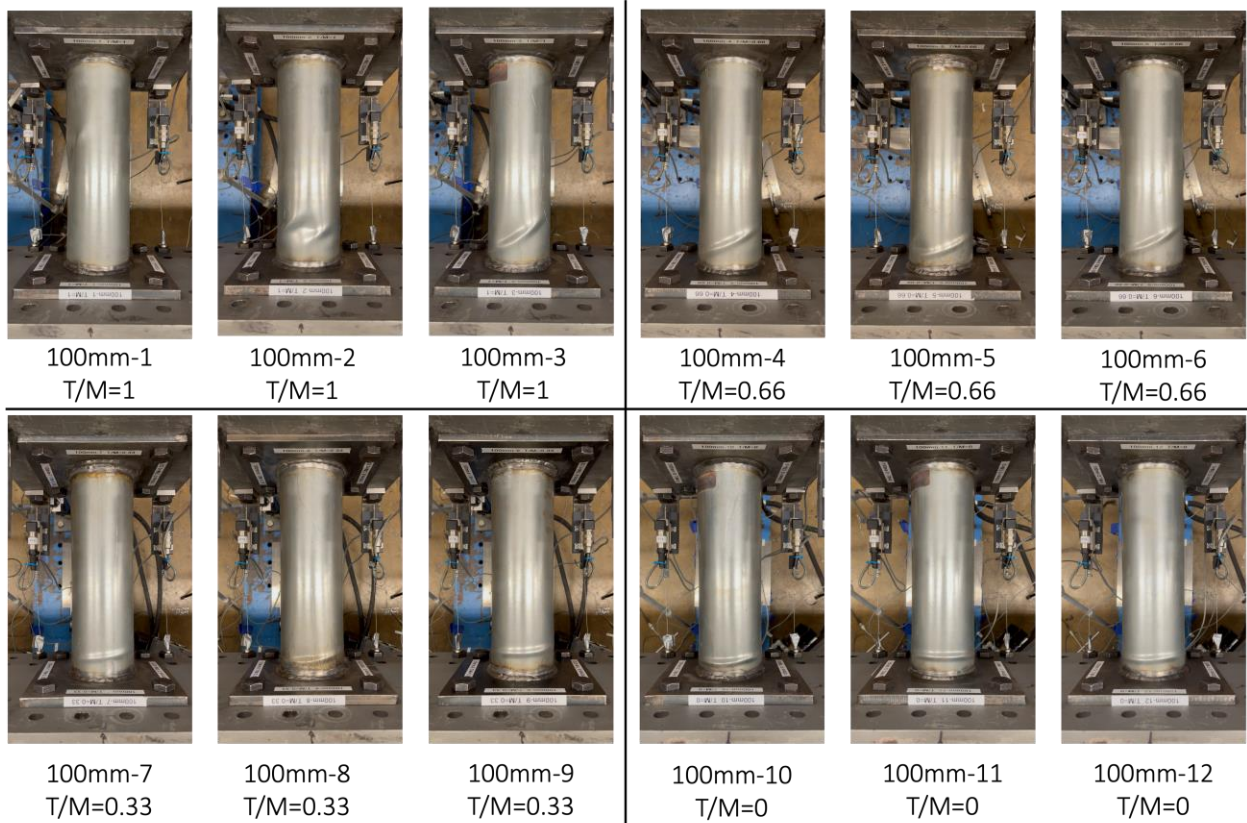


Figure 13: Photos of buckled 100mm tubes

Fig. 14 show results of the 100mm tubes. As D/t ratio decreases, failure occurs more slowly. The load vs displacement plot shows that failure does not happen suddenly for these stockier tubes. After reaching peak load, the load drops slowly instead of the sudden drops seen in the larger tubes. The theoretical bending and torsional stiffnesses match the data well and we have general agreement with Eurocode calculations. The stockiness of these tubes caused the curves for Eurocode predictions to be partially above the von Mises curve in Fig. 14b. This means tubes with low to moderate T/M ratios of this size should fail after reaching yield, which is what happened in these tests.

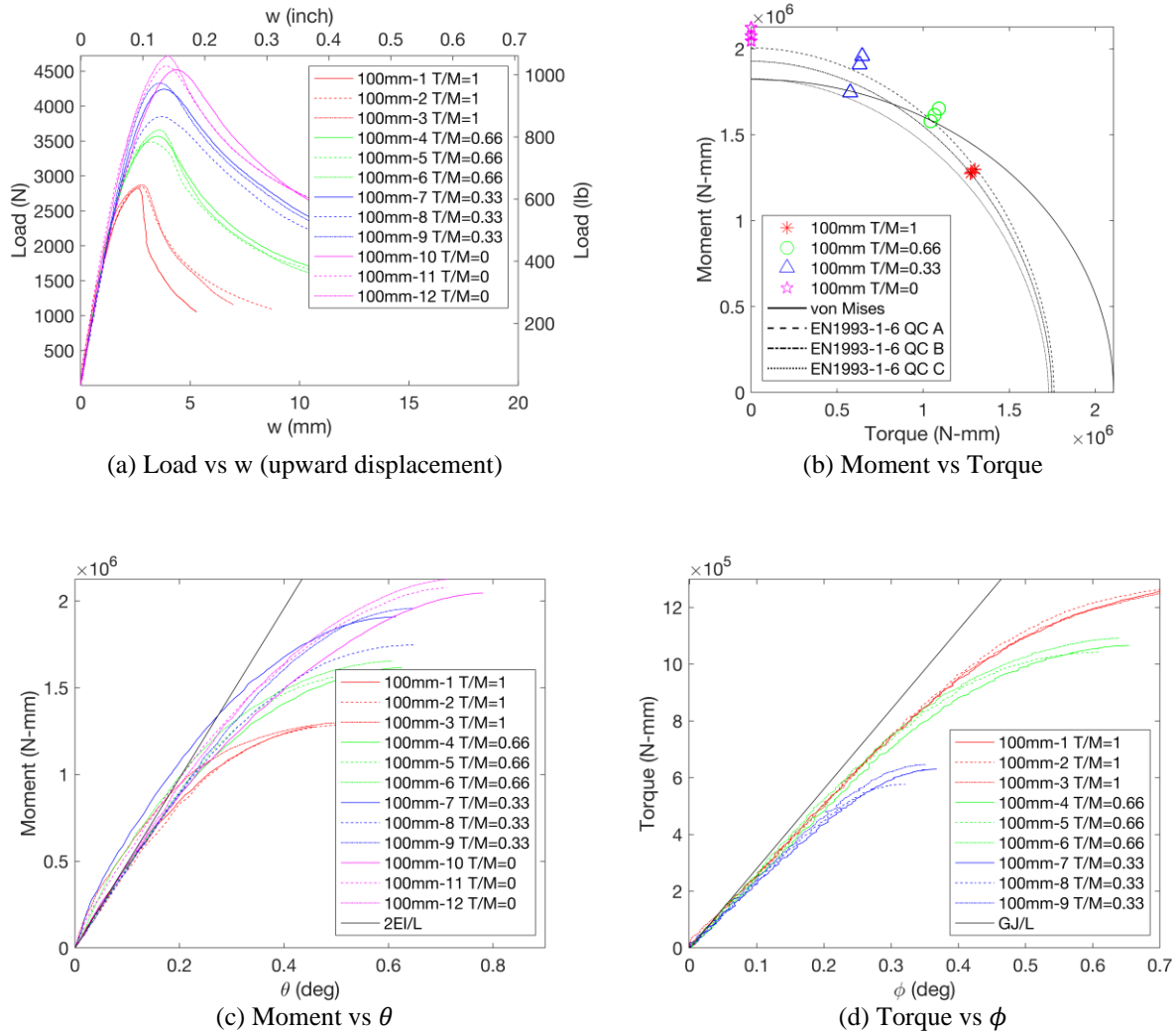


Figure 14: Results of 100mm tubes

6. Conclusions

Wind turbine towers are made from thin cylindrical shells, which have high imperfection sensitivity, making predicting their structural response difficult. The combination of bending and torsion at the top of wind turbine towers is often a controlling load case in design that has not seen significant study to date. The imperfection sensitivity of cylindrical shells in combined bending and torsion also has not been specifically studied. To address this knowledge gap, an experimental study was done on 48 cylinders with diameter-to-thickness ratios ranging from 127 to 320 and bending-to-torsion ratios seen in wind turbine towers. The tubes were first laser scanned to record their actual shape and to gain a better understanding of the resulting imperfection sensitivity. The tubes were then tested under combined bending and torsion, establishing the benchmark strengths. These tests showed that higher diameter-to-thickness ratios result in sudden failures with large drops in load capacity. Adding torsion to bending results in lower load capacities compared with pure bending, and changes the observed buckling and collapse shape in the tube. The test results are in general agreement with Eurocode's interaction formula. Future work will involve assigning Eurocode fabrication quality classes to the tubes and formally assessing reliability, as well as establishing high-fidelity finite element models capable of capturing the buckling strength and failure modes of thin-walled cylinders under different loading scenarios and finally developing reliable and efficient design approaches for such structural elements.

Acknowledgments

This material is based upon work supported by the National Science Foundation under Grant No. 1912481 and No. 1912354. Any opinions, findings, and conclusions or recommendations expressed in this material are those of the authors and do not necessarily reflect the views of the National Science Foundation.

References

- AISC (2000). "Load and Resistance Factor Design Specification for Steel Hollow Structural Sections." Chicago, IL.
- Bruhn, E. F. (1945). "Tests of thin-walled celluloid cylinders to determine the interaction curves under combined bending, torsion, and compression or tension loads." National Advisory Committee for Aeronautics. Report No. 951.
- DNV (2002). "Guidelines for Design of Wind Turbines", 2nd Ed. Det Norske Veritas and Risø National Laboratory.
- Donnell, L. H. (1933). "Stability of Thin-Walled Tubes Under Torsion." National Advisory Committee for Aeronautics. Report No. 479,
- ECCS (2021). Eurocode 3: Design of steel structures - Part 1-6: Strength and Stability of Shell Structures.
- Felton, L. P. and Dobbs, M. W. (1967). "Optimum design of tubes for bending and torsion." *Journal of the Structural Division*, 93, (4) 185–200.
- Gerard, G., Becker, H. (1957) "Handbook of structural stability part III: Buckling of curved plates and shells." National Advisory Committee for Aeronautics. Report No. 3783.
- Hill, R., Siebel, M.P.L. (1951). LXXIII. "On combined bending and twisting of thin tubes in the plastic range." *The London, Edinburgh, and Dublin Philosophical Magazine and Journal of Science*, 42 (330) 722-733.
- Jay, A., Myers, A. T., Torabian, S., Mahmoud, A., Smith, E., Agbayani, N., & Schafer, B. W. (2016). Spirally welded steel wind towers: Buckling experiments, analyses, and research needs. *Journal of Constructional Steel Research* (125), 218-236.
- Nordfab Ducting (2023). <https://nordfabductwork.com/>.
- Rotter, J. M., Schmidt, H. (2013). Buckling of Steel Shells, European Design Recommendations. ECCS - European Convention for Constructional Steelwork.
- Schilling, C. G. (1965). "Buckling strength of circular tubes." *Journal of the Structural Division*, 91 (5) 325–348.
- Schmidt, H., Winterstetter, T.A. (2004) "Cylindrical shells under combined loading: axial compression, external pressure and torsional shear", in Buckling of Thin Metal Shells, eds J.G. Teng & J.M. Rotter, Spon, London, pp 261-285.
- Seide, P., Weingarten, V.I. (1961). "On the Buckling of Circular Cylindrical Shells Under Pure Bending." *Transactions of the ASME*, 112-116.
- Timoshenko, S.P., Gere, J. M. (1961). Theory of Elastic Stability. McGraw Hill (reprinted by Dover in 2009), 541 pp.
- Winterstetter, Th.A., Schmidt, H. (2002) "Stability of circular cylindrical steel shells under combined loading". *Thin-Walled Structures*. Vol. 40 893-909.
- Yamaki, N. (1984). Elastic Stability of Circular Cylindrical Shells, North Holland, Elsevier Applied Science Publishers, Amsterdam, 1984.
- Zhao, X., Tootkaboni, M., Schafer, B.W. (2015). "Development of a Laser-based Geometric Imperfection Measurement Platform with Application to Cold-Formed Steel Construction." *Experimental Mechanics* 55 (9) 1779-1790.